



Preparation, characterization and application of the nanocomposite PCL-PEG-PCL/Bentonite for the removal of methylene blue (MB) dye

Zohra Draoua^{1,2} · Amine Harrane^{1,3} · Mehdi Adjdir^{4,5}

Received: 9 April 2021 / Accepted: 19 July 2021 / Published online: 3 August 2021
© The Author(s), under exclusive licence to Springer Nature B.V. 2021

Abstract

This study focuses on the synthesis, characterization, and application of amphiphilic nanocomposite Poly (ϵ -caprolactone)-Poly (ethylene glycol)—Poly (ϵ -caprolactone) with Bentonite modified PCL-PEG-PCL/Bentonite (A2). The in situ copolymerization was carried out by ϵ -caprolactone and polyethylene glycol in presence of the intercalated Algerian Bentonite tetrabutylammonium hydrogen sulfate (TBHSA) (A1) to obtain a new amphiphilic nanocomposite PCL-PEG-PCL/Bentonite (A2). The nanocomposite was characterized by different techniques including Fourier transform infrared spectroscopy, X-ray diffraction, Transmission electron microscopy, Differential Scanning Calorimetry and thermogravimetric analysis. The nanocomposite (A2) was applied as an efficient removal of methylene blue from aqueous solutions. The effects of the initial pH of a solution, contact time, and nanocomposite mass on the adsorption efficiency were investigated. Pseudo-first/second-order isotherms were applied to determine the efficiency of nanocomposite solid. The experimental data fitted well with the pseudo-second-order model for MB dye adsorption. The mass of nanocomposite increased, the adsorption capacity of dye increases to reach an optimal value at 0.13 g of adsorbent in pH = 6.8. The Langmuir isotherm exhibited the best fit, with an adsorption capacity equal to 600 mg/g.

Keywords ϵ -caprolactone · Nanocomposites · Isotherm · Methylene blue · Bentonite

✉ Zohra Draoua
z.draoua@univ-usto.dz

✉ Mehdi Adjdir
Mehdi.adjdir@daad-alumni.de

Extended author information available on the last page of the article

Introduction

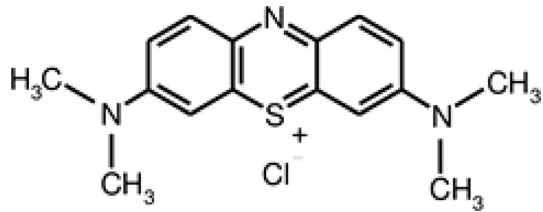
Contamination of wastewater by different forms of pollutants is a real problem. Among these pollutants the dyes, which are considered potentially toxic compounds and harmful to the environment [1]. Different industries such as textile, pulp, paper, printing, food, plastic, and tanneries commonly use organic dyes that are aromatic compounds [2]. These dyes can easily be transported in the aqueous environment due to their high solubility in water and therefore can present many serious ecological, environmental and health risks [3]. Various conventional methods have been proposed for the removal of dyes from wastewater by using phyllosilicate [4, 5] zeolites [6], HDLs [7], polymers [8], magadiite [9] and hybrid nanomaterials [10, 11]. The hydrophobic nature of PCL in water systems leads to the stability of its chemical and mechanical properties, favoring its use in aqueous media. On the other hand, PCL leads to the modification of the Bentonite character from hydrophilic to hydrophobic. Despite the large investments in biodegradable polymers, it is evident that they are still far from becoming alternatives to the conventional non-degradable polymers for examples: Linear high-density polyethylene (HDPE), Branched low-density polyethylene (LDPE) widely used. In general, the main limitations are due to expensive manufacturing costs and disadvantageous physical properties (e.g., poor mechanical and thermal properties, high hydrophobicity, and poor process ability) [12, 13]. Therefore, it seems very necessary to change their chemical nature and/or enhance their performance by nanotechnology. The addition of phyllosilicates into a polymer phase leads to polymer/phyllosilicates composites with enhanced properties. Although there are several elaboration methods developed, the in situ polymerization of monomers mixed with layered silicates seems to be the most suitable way for obtaining either intercalation or the exfoliated structures. This method should have a greater impact on properties than micro-composites [14–21]. In recent years there has been a growing interest in the use of clay minerals such as Bentonite, kaolinite, diatomite and fuller's earth as adsorbents not only to separate inorganic but also organic molecules, this is demonstrated by several researchers [21–24]. In the literature, no work has been reported on the use of PCL-PEG-PCL/Bentonite-TBHSA (A2) as an effective dyes adsorbent. In this work, the structural, morphological, thermal properties and application as an efficient adsorbent of A2 have been extensively studied under different adsorption parameters.

Experimental

Materials

ϵ -Caprolactone (grade 99%), polyethylene glycol(PEG) (Mn: 2000 $I=1.2$) and TBHSA have been supplied by Aldrich Chemicals, Tetrahydrofuran (THF), Dichloromethane and methanol were dried over $MgSO_4$ and distilled.

Fig. 1 Structural formula of the MB dye



Tetrabutylammonium hydrogen sulfate was used as purchased from Aldrich. Bentonite: clay, was procured from (Algerian Society of Bentonite) BENTAL.

Methylene blue (MB), is an organic cationic molecule belongs to the family of Xanthenes of the chemical formula $C_{16}H_{18}C_1N_3S$ [25]. It possesses a molar mass of 319.86 g/mol and a solubility of 50 g/L and 10 g/L at 20° C in water and ethanol, respectively. Also, it is known as methylthionium chloride or bis (dimethylamino) -3,7 phenazathionium chloride. Figure 1 shows structural formula of the MB dye.

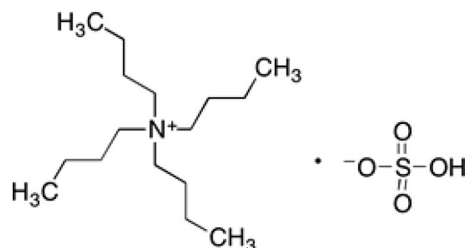
Preparation of bentonite- Na^+

100 g of Bentonite was dispersed in 1L of 1 M aqueous solution of $NaPO_3$. The suspension was kept under stirring for 2 h and then allowed to stand for 24 h in 2L cylinder. The dispersed < 2 μm Bentonite- Na clay was collected from the suspension and was then separated by centrifugation under 4500 rpm for 1 h then dried at 150 °C under vacuum [26–28].

Organic modification of bentonite (A1)

Bentonite- Na (10 g) was dispersed in 50 ml distilled water and combined then with 50 ml of 2 M tetrabutylammonium hydrogen sulfate (TBHSA) aqueous solution. Figure 2 shows structural formula of TBHSA. The mixture was kept under magnetic stirring for 3 h at room temperature. The composite was then filtered, washed until eliminate the sulfate anions. The physisorbed butyl ammonium cations were removed by washing the composite with a pre-heated water/ethanol mixture 50:50. The resulting A1 exchanged with butyl ammonium cations was dried at 50 °C under vacuum. The organophilic Bentonite produced was dried at 120 °C and crushed and is called Bentonite-TBHSA (A1).

Fig. 2 Structural formula of the TBHSA



Synthesis of nanocomposite A2

The Poly (ϵ -caprolactone) -poly (ethylene glycol)—poly (ϵ -caprolactone)/(bentonite-TBHSA)nanocomposite noted (A2)is synthesized by the in-situ copolymerization of ϵ -caprolactone with poly (ethylene glycol) catalyzed by bentonite-TBHSA(A1).

In one flask immersed in a temperature-controlled bath at 80 °C, A1 is maintained under vacuum before the introduction of 1 g of ϵ -caprolactone and kept under stirring, after 3 h 0.34 of PEG2000 was added. After several hours, the reaction was cooled and stopped, then washed with methanol, the obtained product was called nanocomposite A2. A2 was kept in vacuum at 40 °C before weighing.

Characterization of nanocomposites A2

Structure, morphology and thermal stability of nanocomposites A2 were analyzed by X-ray diffraction (XRD), transmission electron microscopy (TEM), FT-IR, thermogravimetric Analysis TGA and DSC. XRD diffractograms for pressed powder samples were recorded on a Philips PW 1710 diffractometer using Cu-K α radiation ($\lambda = 1.5406 \text{ \AA}$). D-spacings were calculated according to Bragg's law. TEM images were performed with a Philips CM100 apparatus using an acceleration voltage of 100 kV. Ultrathin sections of nanocomposites (80 nm thick) were prepared at $-130 \text{ }^\circ\text{C}$ with a Reichert-Jung Ultracut 3E, FC4E ultracryomicrotome equipped with a diamond knife. Because of the large difference in the electron density between silicate and polymer, no selective staining was required to observe the internal structure [29]. Differential Scanning Calorimetry (DSC) was performed under nitrogen flow ($75\text{cm}^3/\text{min}$) at a heating rate of $10 \text{ }^\circ\text{C}/\text{min}$ from room temperature to $200 \text{ }^\circ\text{C}$ with a Perkin Elmer Instrument DSC6 thermal analyzer. Fourier Transform infrared (FTIR) spectra were recorded between 400 and 4000 cm^{-1} on Perkin -Elmer B25 spectrometer. Thermal analysis (TG) was performed in air, and all the samples were heated to $1000 \text{ }^\circ\text{C}$ at heating rate of $10 \text{ }^\circ\text{C min}^{-1}$.

Experimental procedure

The experimental study dye adsorption was carried out in synthetic dilute solutions of methylene blue in batch, by dissolving a specific adsorbent mass in a known concentration solution of MB, during a set time. After this time, the liquid phase is recovered and filtered, and the dye residual concentration was determined from the absorbance analysis (A) which were followed using UV-Visible spectrophotometer, type 2401 PC, at $\lambda_{\text{max}} = 675 \text{ nm}$. The adsorption equilibrium was achieved by varying; initial dye concentration, $1\text{--}100 \text{ mg/L}$; contact time, from 0 to 210 min; mass of the adsorbent, from 20 to 355 mg; pH, $1\text{--}10.2$ and ambient temperature of $25 \text{ }^\circ\text{C}$. The percentage of the discoloration R(%) and q_e amount of dye adsorbed (mg/g) of the MB were calculated using the following equations, respectively:

$$\% \text{ adsorption} = \frac{(C_i - C_{eq}) 100}{C_i} \quad (1)$$

$$q_e = \frac{X}{m} = \frac{(C_i - C_{eq}) V}{m} \quad (2)$$

where C_i is the initial concentration (mg/L), C_{eq} is the equilibrium concentration (mg/L), V is the volume of the solution (L), m is the mass of adsorbent used (g), and X number of grams of MB adsorbed (mg).

Structural and morphological properties of amphiphilic nanocomposite A2

The XRD patterns of Bentonite-Na, TBHSA–Bentonite (A1), and nanocomposite (A2) are shown in Fig. 3. The powder XRD pattern of Bentonite-Na was assigned to the typical pattern of phyllosilicates Bentonite material with several (001) reflections. The main (001) reflection presents a basal spacing of 12.86 Å. This pattern fits well with the pattern of Na-Bentonite reported in the Powder Diffraction File under the JCPDS Card No. 003–0019 and is in very good agreement with earlier works [10, 26, 27]. After intercalation with TBHSA, the basal spacing, d_{001} , of the resulting product becomes bigger to reach 14.56 Å; indicating the successful intercalation method. Indeed and based on the basal spacing, we can assumed that the TBHSA is intercalated as monolayer within the Bentonite layers, this is because of its alkyl chains which are very short (4 carbons). The d_{001} of the Bentonite TBHSA (A1) seems to be highly increased after in-situ copolymerization by caprolactone and ethylene glycol to reach 20.01 Å. Based on the enhancement of the basal spacing after

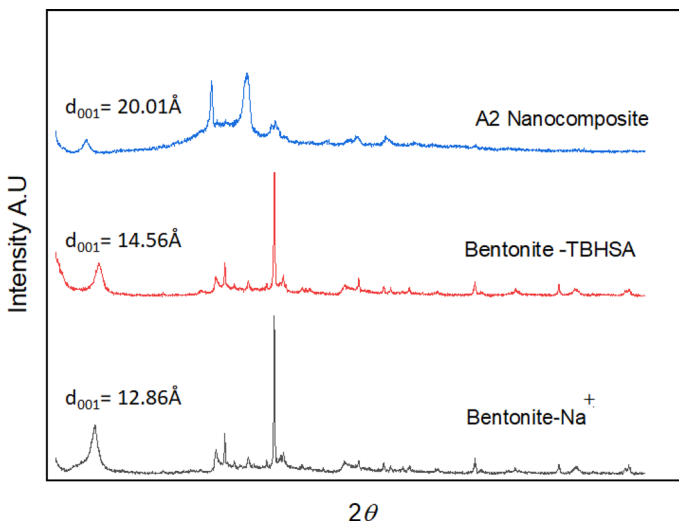


Fig. 3 XRD patterns of bentonite- Na^+ , bentonite -TBHSA, and nanocomposite A2

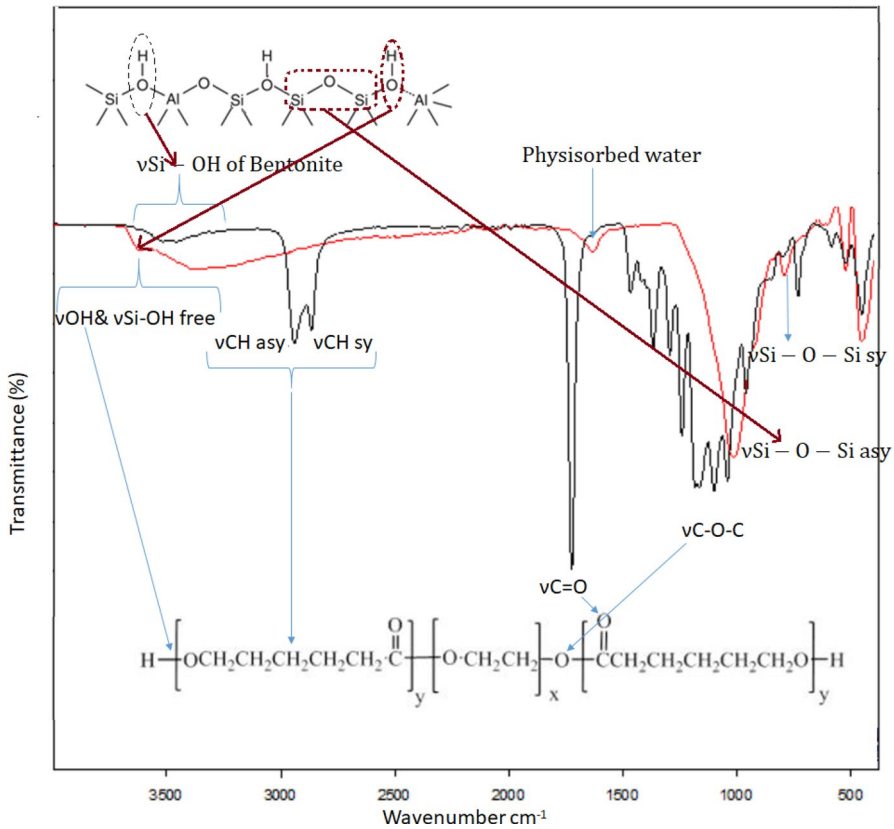


Fig. 4 Exhibits the IR functional bands of bentonite- Na^+ and nanocomposite A2

in-situ copolymerisation where the d_{001} increased from 12.86 to 20.01 Å, it can be assumed that the copolymers are arranged in the interlayer space with paraffin type structure.

Based on XRD, the amphiphilic nanocomposite (A2) exhibits a decrease in the intensity of the main peak that characterizes Bentonite in the region of small angles for both samples, indicating the formation of a partially exfoliated/partially intercalated structure. [15, 16, 23].

The FT-IR spectra of Bentonite- Na and nanocomposite A2 are displayed in Fig. 4. The results demonstrated that the absorption band at 3619 cm^{-1} is related to OH groups either of PCL blocks or to isolated Si-OH of Bentonite [30, 31]. The broad absorption band ranged between 3536 and 3395 cm^{-1} is attributed to the vibrations of OH groups implied in strong interlayer hydrogen bands, Si-OH, as well as to the interlayer water molecules. The peak of C-H stretching appeared at 2947 cm^{-1} and 2877 cm^{-1} , which proved the existence of PCL blocks in the copolymer. A Stretching vibration of the ester carbonyl group (C=O) of PCL

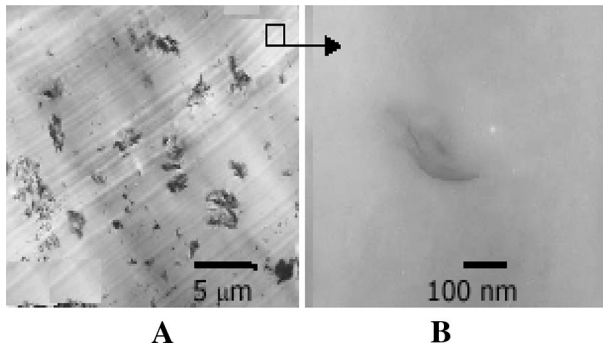


Fig. 5 TEM microscopy images for A2 nanocomposite

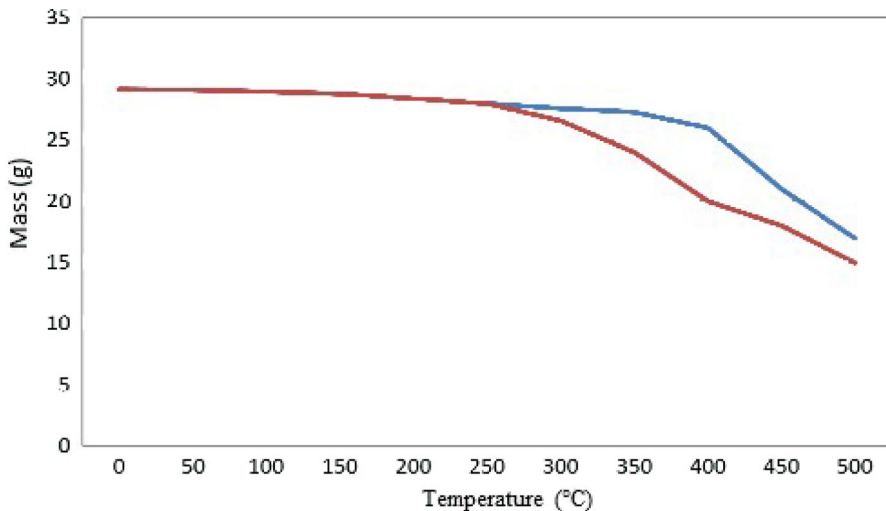


Fig. 6 Thermogravimetric Analysis of nanocomposite A2- and copolymer pur -

blocks appeared at 1736 cm^{-1} . The bands at $1250\text{--}1100\text{ cm}^{-1}$ are associated with the C–O–C stretching vibrations of the $-\text{OCH}_2\text{CH}_2-$ of PEG blocks. The pic at 1670 cm^{-1} is attributed to the OH of water physisorbed.

Figure 5 shows the TEM image of the A2 nanocomposite. This observation suggests that the fillers were mostly homogeneously distributed in the PCL-PEG-PCL matrix.

It is observed in Fig. 6. that at temperatures above $400\text{ }^\circ\text{C}$, the A2 mass decreases. This phenomenon could be assigned to the degradation of the copolymer due the high temperature. However, the A2 nanocomposite presents an enhancement in the thermal stability from $300\text{ }^\circ\text{C}$ of pur copolymer PCL-PEG-PCL [32] to $400\text{ }^\circ\text{C}$, this improvement is due to the Bentonite framework. The hydrophobic character of nanocomposite A2 has been proven by the absence of any mass loss in the range of $80\text{--}150^\circ\text{C}$ Fig. 6.

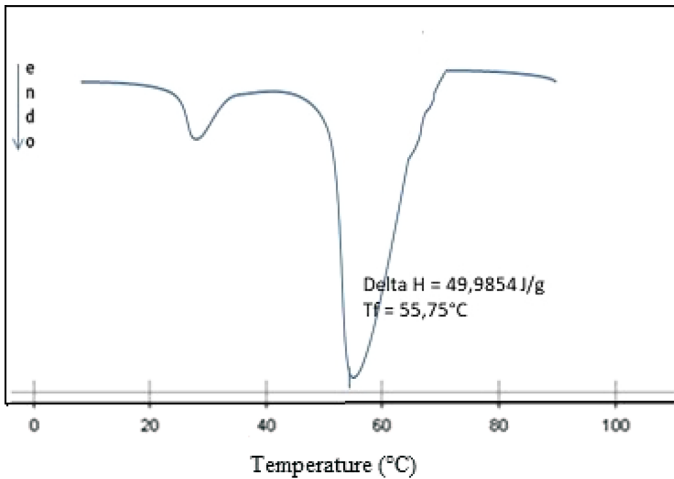


Fig. 7 DSC thermograms of A2 nanocomposites

The DSC analysis was performed to study the influence of the loading rate of A1/polycaprolactone on the T_g of the nanocomposite A2 Fig. 7. The T_g of the A2 nanocomposites appears in the range of (-59 °C) and (-57 °C). This increase of about 15 °C compared to PCL-PEG-PCL is due to the introduction of clay into the matrix which makes it more rigid. Furthermore, on the thermogram of the A2 nanocomposite, we also observe the presence of a second endothermic peak between (35) and (50) °C for different loading rates, which indicates the removal of water physisorbed. The evolution of the crystallinity of the resulted A2 nanocomposites was also studied by DSC measurements. The degree of crystallinity is proportional to the melting enthalpy of the material. As shown in Fig. 7, the crystallinity of the resulted nanocomposites, expressed by the melting enthalpy ΔH_m of polycaprolactone segment in the copolymer, increases with high contents of A1. It is known that two processes govern the polymer crystallization, nucleation, which is the mobility of polymer segment to a growing crystal face, and diffusion, the formation of new layers on the crystal [33–37].

MB dye adsorption

MB dye Adsorption onto different materials is frequently described as a process in order to depend on different parameters specially reaction time which may give many information on the yield and the kinetic adsorption process [38]. In order to investigate the effect of contact time on the elimination of methylene blue, a series of experiments was performed using the following protocol: 0.13 g of adsorbent in 50 mL solution with initial concentrations of methylene blue: 10 mg/L at ambient temperature.

Figure 8 shows the adsorbed amount of MB dye with contact time. The kinetic study of the elimination of MB dye by the adsorbent material shows an increase in the adsorbed amount with the increase in contact time.

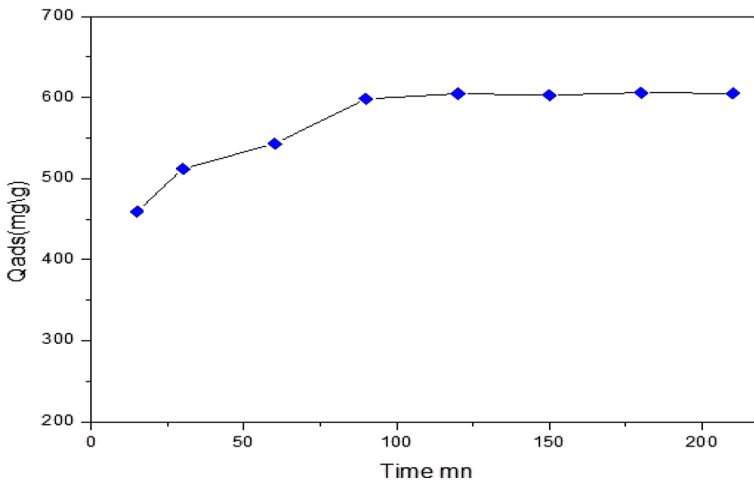


Fig. 8 Kinetics of adsorption of MB on A2 nanocomposite

It is observed that the maximum adsorption is attained with adsorption capacity of MB dye is around 600 mg/g within 90 min. In fact, the dye molecules are adsorbed in the first place on the easily accessible sites, a diffusion of these molecules toward the less accessible adsorption sites takes place as the agitation is carried out until reaching the equilibrium value within 90 min. The elimination of MB stabilization (saturation) after the fixed reaction time between this nanocomposite and MB dye depends on the availability of active and vacant adsorption sites at the surface of the nanocomposite [39]. However, no significant changes were remarked in the removal rate of the MB dye after equilibrium. Similar results have been reported for adsorption of Methylene Blue on activated thermally clays at 500 °C, the adsorption rate was higher at 89% about 90 min [40]. To evaluate the efficiency of this material as adsorbents of MB dye, adsorption capacities between this material in this study and various adsorbents. However, the other results were reported for the adsorption of MB. Batch adsorption equilibrium experiments indicated that the adsorbed amount of BM dye by sodium clay was about 330 mg/g with a rapid initial step and reach equilibrium within 20 min [41] Also, Dhananasekaran et al. studied the adsorption MB dye by α -Chitin Nanoparticles [5]. The adsorption process achieved maximum at adsorbed amount about 6.9 mg/g within 30 min.

Effect of adsorbent mass

The effect of the adsorbent mass was studied by varying the adsorbent amounts from 0.1 to 0.25 g for the initial dye concentration of 20 mg/L at pH of MB dye solution within 90 min.

Figure 9 shows that the adsorbed quantities of discoloration increased considerably as the mass of nanocomposite increased, it reaches an optimal value at 0.13 g then decreases. The optimal amount of the adsorbed dye is very high as it reaches

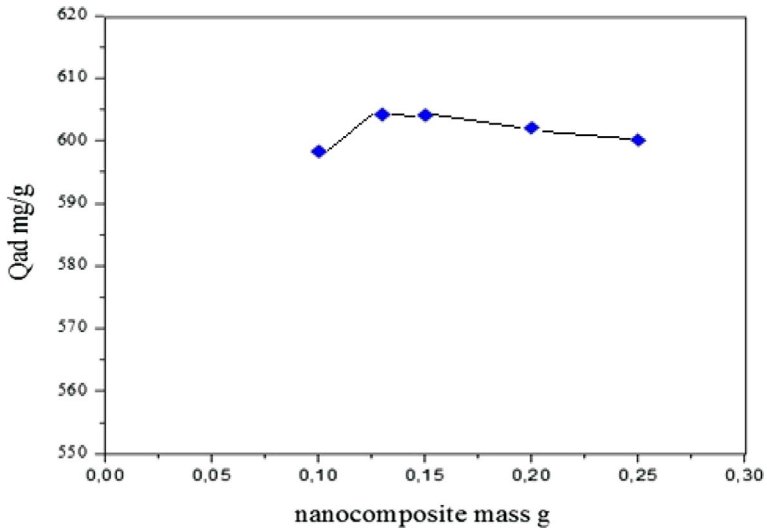


Fig. 9 Effect of adsorbent mass on adsorption of MB

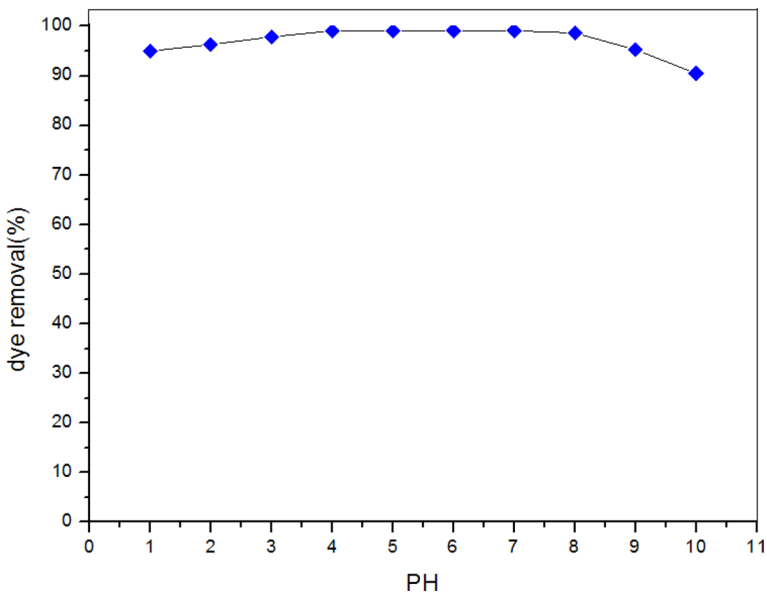


Fig. 10 Effect of pH on adsorption of MB

14.2 mg/g. This result can be explained on the probable availability of more free reactive sites for nanocomposite to interact with dye species.

Effect of solution pH on MB uptake

pH of the aqueous solution, is an important parameter that affects the dye adsorption behavior [5]. Indeed, the adsorption behavior of MB dye on nanocomposite has been studied over a wide range of pH 1–10.2 by adding HCl or NaOH to adjust the desired pH value. The results illustrated at Fig. 10 show that the removal rate of the dye is slightly influenced by the pH changes. However, it can be adsorbed at acidic and basic pH.

The obtained results revealed a rather increase in MB removal with the pH, reached the maximum from pH=4 to the initial pH solution of MB pH=6.8, therefore it decreased slightly with a lowering up to 10% at basic medium. The maximum adsorption is attained the maximum dye removal efficiency about 98% at the initial pH solution of MB pH=6.8. Nevertheless, the variation of the level of influence of the solution pH on the MB dye adsorption efficiency depends on the adsorbent–adsorbate interaction [39]. The dye adsorption was attributed to the hydrophobic–hydrophobic interaction between hydrophobic groups of PCL-PEG-PCL molecules and cationic dye as the carbon chain C16 and the sulfonate groups. Indeed, many investigations were reported using other adsorbents such as: activated carbon from vegetable sponge of cylindrical loofa [42] wheat shells [43] and clay [44]. In an acid medium, the H⁺ ions are very mobile and might occupy the free active sites of the nanocomposite surface or can be also attracted by the different active sites of MB dye, namely S and N [45]. Nevertheless, there are alternative ions competing between H⁺ ions and MB dye species. Also, the surface of the nanocomposite based clay becomes positive charged which creates more free reactive sites and a combined interaction with MB dye species and this leads to encourage its adsorption effectiveness.

This statement is confirmed by the high removal efficiency at lower pHs. At high pH, the surface of nanocomposite can be deprotonated and typically create negative charge. Thus, it is advantageous that the process is a suitable application for MB dye removal because of its neutral and clean effluent [39]. However, the initial solution pH of 6.8 was chosen for the rest of the experiments on MB dye adsorption.

Kinetic adsorption study

Kinetic study has prime importance in dye adsorption process because it acquires the rate efficiency of adsorption with respect to time and also describes the mechanism of adsorption between the adsorbate and the adsorbent [43].

The adsorption kinetics was investigated by following of methylene blue concentrations with respect to time. Indeed, two models were applied to describe the adsorption kinetics mechanism of methylene blue. The experimental data were fitted to the Lagergren first-order kinetic model (Eq. 3) and pseudo-second-order kinetic model (Eq. 4) as follows [40]:

$$\ln (q_e - q_t) = \ln(q_e) - (K_1)t \quad (3)$$

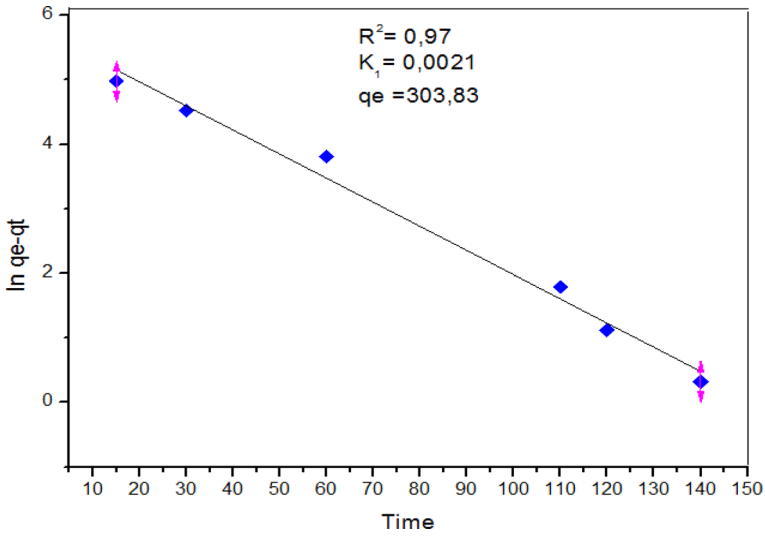


Fig. 11 Pseudo-first order for the adsorption of MB on A2 nanocomposite

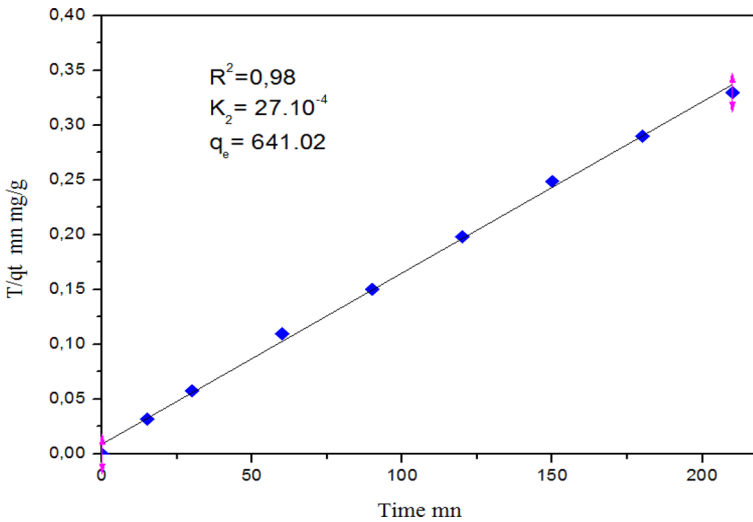


Fig. 12 Pseudo-second order for the adsorption of MB onto A2 nanocomposite

$$\frac{t}{q_t} = \left(\frac{1}{K_2 q_e^2} \right) + \left(\frac{1}{q_e} \right) t \quad (4)$$

where q_t and q_e are the amount of adsorption at time at equilibrium (mg/g), respectively; k_1 is the constant rate of pseudo-first order (1/min); k_2 is the constant rate of pseudo-second order (g/(mg min)). The application of linear form of the pseudo-second-order equation for the MB dye adsorption onto this nanocomposite is depicted

Table 1 Kinetic models for MB dye adsorption onto composite

Adsorbate and adsorbent	C_0 (ppm)	q_e (mg/g) calculée	Pseudo-first order		Pseudo-second order			
			$q_e^{(exp)}$ (mg/g)	K_1	R_1^2	$q_e^{(exp)}$ (mg/g)	K_2	R_2^2
Nanocomposite-methylen blue	10	600	303.83	0.0021	0.97	641.02	27.10^{-4}	0.98

in Figs. 11 and 12. The kinetic constant rates K_1 , K_2 and the amount of adsorption at equilibrium q_e were determined from the slope and intercept of the corresponding linear forms, respectively.

The results obtained from Table 1 show that the data kinetic adsorption calculated from pseudo-first-order model is not valid to describe the MB dye species mechanism adsorption by A2 nanocomposite. However, it observed also that the pseudo-second order is the mostly suitable to fit the experimental data than pseudo-first order, since its correlation coefficients are higher than those of the first–second-order model. However, it was found that the kinetic constant rate K_2 was of 106 g/mg.h and correlation coefficient of 0.98. Indeed, the experimentally adsorbed quantities at equilibrium mg/g were found to be in good agreement with those calculated from the second-order reaction kinetics Eq. (641 mg/g). These obtained results are in agreement with similar trends previously recorded for MB dye removal by thermally activated clays [40] and activated carbon from vegetable sponge of cylindrical loofa [42].

Adsorption isotherm study

To evaluate the adsorbed amount capacity of the adsorption isotherm with various initial concentrations of MB dye ranging from 5 to 30 mgL⁻¹. The adsorption isotherm nonlinear has been determined by plotting the relation of q_e as a function of C_{eq} Fig. 13.

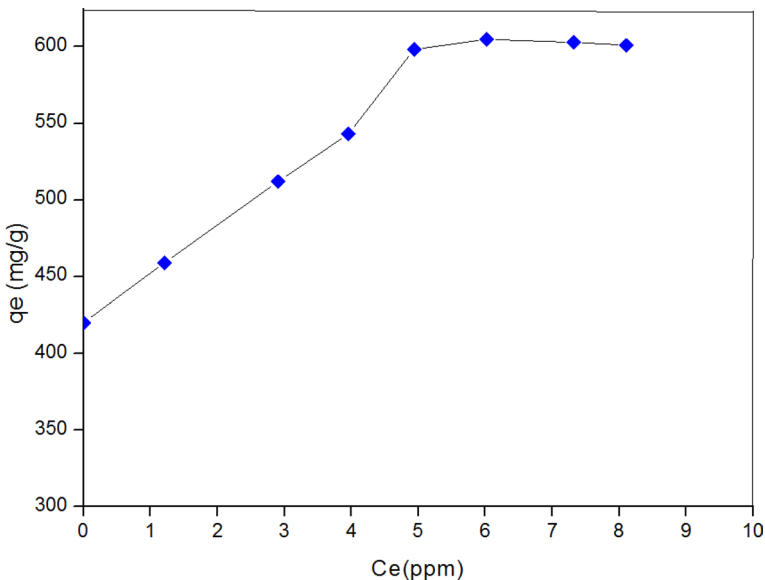


Fig. 13 Adsorption isotherm of the MB onto A2 nanocomposite

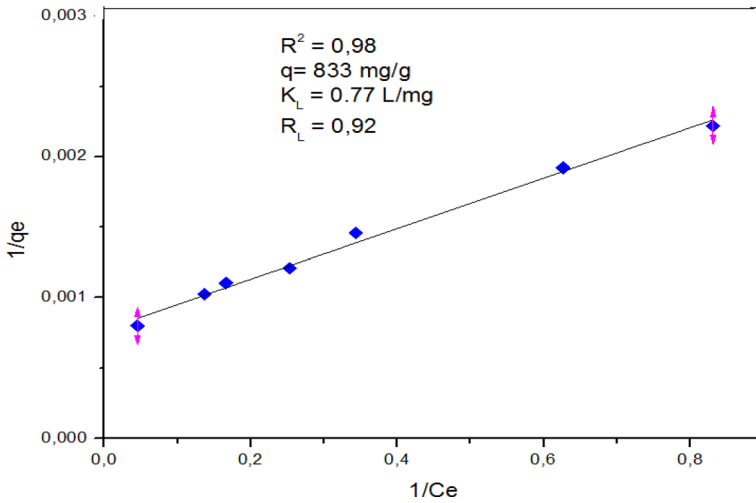


Fig. 14 Transformed linear Langmuir isotherms for adsorption of MB on A2 nanocomposite

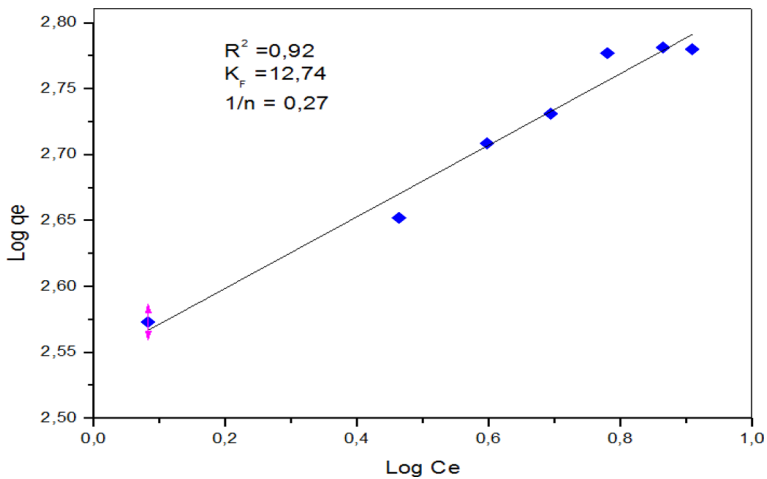


Fig. 15 Transformed linear Freundlich isotherm for adsorption of MB on A2 nanocomposite

Figure 13 shows that the adsorption capacity increases with the initial concentration. The recorded highest adsorbed amount at equilibrium of MB dye was observed about 600 mg/g.

The isotherm shows almost steady state value indicating the saturation of the adsorbent surface and then formation of a monolayer. These isotherms are of type *L* in the classification of Giles and all [39, 46, 47].

This corroborates with similar findings in the case of methylene blue adsorption on a copper montmorillonite and thermally activated clays [40, 41].

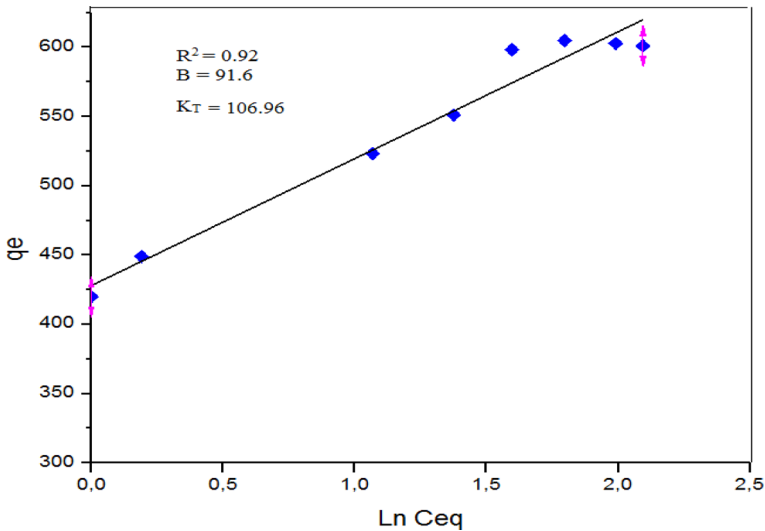


Fig. 16 Transformed linear Temkin isotherm for adsorption of MB on A2 nanocomposite

Langmuir, Freundlich and Temkin isotherm models were applied to assess the dye adsorption phenomena onto this nanocomposite.

The Langmuir isotherm model is the most widely used to present liquid—solid adsorption which assumes monolayer adsorption, Whereas, Freundlich model is empirical which assumes the heterogeneous adsorption on the surface [48, 49]. However, Temkin model assumes that the decrease in heat of adsorption with recovery rate is linear rather than logarithmic [31, 39, 48].

The linear form of Langmuir, Freundlich and Temkin isotherm models was presented in Figs. 14, 15 and 16 which can be determined by the following relations [40].

$$\frac{C_{eq}}{q_e} = \frac{1}{K_L q_m} + \frac{C_{eq}}{q_m} \quad (5)$$

$$\text{Log } q_e = \text{Log } K_F + \frac{1}{n} C_{eq} \quad (6)$$

$$q_e = B \ln K_T + B \ln C_e \quad (7)$$

where $B = RT/b$ and C_e : The equilibrium concentration (mg/L), q_e : The amount adsorbed per gram of adsorbent (mg/g), K_L : Langmuir constant (L/mg), K_F : Freundlich constant (L/mg), q_{max} : maximum adsorbed amount per gram of adsorbent (mg/g), n : Freundlich constant characteristic of the effectiveness of adsorbents toward given solutes, B : Temkin constant for heat of adsorption, K_T : Adsorption equilibrium constant corresponding to the maximum binding energy [50].

The isotherm parameters K_L , K_F , n , K_T and B and correlation coefficients (R^2) for each model are regrouped in Table 2.

Table 2 Parameters of the adsorption isotherms studied for the A2 nanocomposite

Isotherm model	A2 nanocomposite
<i>Langmuir</i>	
q_m (mg/g)	833
K_L	0.77
R_L (L/mg)	0.92
R^2	0.98
<i>Freundlich</i>	
K_F	12.74
$1/n$	0.27
R^2	0.92
<i>Temkin</i>	
B	91.60
K_T	106.96
R^2	0.925

R_L is an important characteristic of the Langmuir isotherm which expressed a dimensionless constant, called equilibrium parameter and determined by the following equation:

$$R_L = 1 / (1 + K_L * C_0) \quad (8)$$

An equilibrium parameter $R_L > 1$ shows that the adsorption is unfavorable, if $R_L = 1$ the adsorption is in linear form, the adsorption can be favorable when $0 < R_L < 1$, and a zero separation factor ($R_L = 0$) indicates that adsorption is irreversible [39].

Based on the data obtained from Table 2, the application of the linearized forms of Langmuir, Freundlich and Temkin laws is made to verify which model is valid for modeling the adsorption isotherms in the interval of the studied concentrations. The obtained correlation coefficients ($R^2 = 0.99$) of Langmuir equations are much better to fit the experimental data than those of Freundlich and Temkin, indicating that the adsorption data were well described by Langmuir isotherm model and obeyed to monolayer molecule adsorption. In addition, the calculated data of equilibrium parameter R_L from the Langmuir model were about 1, indicating favorable adsorption of MB dye by the adsorbent.

In conclusion, the probable formation of a monolayer of MB dye homogeneously on surface of A2 nanocomposite, without any mutual interactions between localized sites whose energy is identical. Additionally, the maximum adsorption capacity for MB dye molecules by A2 nanocomposite given by Langmuir was about 800 mg/g Table 2, which was close to obtained experimental value.

These results agreed with those previously reported for removal MB dye removal by sodium clay [51], mucuna beans [38], and microporous Cu-doped BTC (Cu-BTC) metal-organic composite materials [39].

Table 3 Comparison of maximum adsorption capacity at equilibrium (q_e) of nanocomposite A2 with different adsorbents

Adsorbent	q_e (mg/g)	References
Montmorillonite sodium (AS)	240	[40]
Montmorillonite calcium (AC)	450	[40]
Montmorillonite clay(CC 300 °C)	224	[41]
Montmorillonite clay(CC 500 °C)	124	[41]
Activated carbon	232.5	[52]
Chemically modified GNPs	225	[53]
Activated carbon (AC)	476.88	[54]
Chitosan-microspheres (CMMS)	371.7	[55]
Fe ₃ O ₄ @SiO ₂ -(CH ₂) ₃ -IL/Talc	6.23	[56]
microporous Cu-doped BTC (Cu-BTC) metal-organic composite	189.12 (20 °C)	[39]
Nanocomposite A2	600	This study

Comparative study of MB dye adsorption on different materials

To assess the performance and adsorption efficiency of the synthesized nanocomposite based clay as an appropriate adsorbent for MB dye in aqueous solution is necessary to apply the in situ polymerization that polymer can be added to phyllosilicates by intercalation into the interfoliar space, and this leads thereafter to produce polymer/phyllosilicates nanocomposites with enhanced adsorptive properties.

The comparison of maximum adsorption capacities (q_e) of the MB dye on different types of adsorbent from aqueous solution was summarized in Table 3. Overall, it can be noticed that this nanocomposite based clay is mainly low-cost adsorbent with different adsorptive properties and could be used in large scale to remove

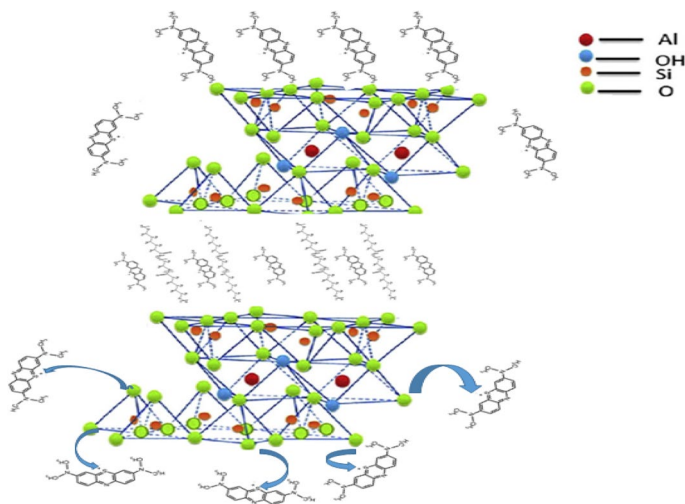


Fig. 17 The possible interaction mechanism proposed between nanocomposite A2 and methylene blue

successfully MB dye. The adsorption capacity of MB dye on A2 nanocomposite is higher compared with the other adsorbents such as activated carbon, chitosan-microspheres and different other types of clays Table 3. It can be suggested that A2 nanocomposite is a promising material for the efficient removal of dyes from aqueous solution.

Adsorption mechanism

Based on the pH section, the adsorption mechanism of methylene blue dye is split into two phenomena Fig. 17.

- (i) The hydrophobic interaction between the dye and the hydrophobic block (PCL) of the copolymer.
- (ii) The electrostatic interaction between the Si–O-, and Al–O- surface and edge groups of Bentonite and the sulfonic group of dye.

Conclusion

PCL-PEG-PCL/Bentonite A2 nanocomposites have been prepared by in situ ring-opening polymerization of ϵ -caprolactone, in the presence of PEG chains, catalyzed by a Bentonite. For this purpose, Bentonite- Na^+ has been exchanged by tetrabutylammonium cations. X-ray diffraction and transmission electron microscopy show the partially exfoliation of the silicate sheets in the PCL-PEG-PCL triblock copolymer/layered silicate nanocomposites. The resulted A2 nanocomposites display good mechanical properties and a high adsorption capacity of dye. The maximum adsorption capacity of MB dye is about over 600 mg/g within 90 min. It is also noticed that when the mass of A2 nanocomposite increased, the adsorption capacity of dye increases to reach an optimal value at 0.13 g of adsorbent in $\text{pH}=6.8$ and ambient temperature. The Langmuir isotherm was found to be the most suitable model to represent the adsorption of the MB dye; the regression data show a good correlation between the Langmuir isothermal model and the obtained experimental results. For kinetic study, the experimental data fitted well with the pseudo-second-order model for MB dye adsorption.

Acknowledgements The authors gratefully acknowledge the scientific support from Pr; Amina Ramdani, Department of Science, University Dr. Moulay Tahar, Saïda Algeria.

References

1. J.N. Tiwari, K. Mahesh, N.H. Le, K.C. Kemp, R. Timilsina, R.N. Tiwari, K.S. Kim, *Carbon* **56**, 173 (2013)
2. G. Moussavi, M. Mahmoudi, J. Hazard, *Mater* **168**(2–3), 806 (2009)
3. G. Moussavi, M. Mahmoudi, *Chem. Eng.* **152**(1), 1 (2009)
4. C.L. Young, J.K. Eui, Y. JiW, J.S. Hyun, *J. Hazardous, Materials* **192**(1), 62 (2011)

5. A. Kadeche, A. Ramdani, M. Adjdir, A. Guendouzi, S. Taleb, M. Kaid, A. Deratani, *Res. Chem. Intermed.* **46**, 4986 (2020)
6. D. Karadag, E. Akgul, S. Tok, F. Erturk, M.A. Kaya, M. Turan, *Chem. Eng. Data* **52**(6), 2436 (2007)
7. M. Kute, H. Deo, *PharmaInnovat* **7**, 190 (2018)
8. A. Mishra, R. Srinivasan, M. Bajpai, R. Dubey, *Colloid. Polym. Sci.* **282**, 722 (2004)
9. M. Boudahri, D. Bouazza, M. Adjdir, H. Miloudi, N. Abdelkader, A. Tayeb, *Res. Chem. Intermed.* **44**, 6105 (2018)
10. Z. Cai, Y. Sun, W. Liu, F. Pan, P. Sun, J. Fu, *Environ. Sci. Pollut. Res.* **24**, 15882 (2017)
11. R. Cherrak, M. Hadjel, N. Benderdouche, M. Adjdir, A. Mokhtar, K. Khaldi, A. Sghier, P.G. Weidler, *SILICON* **12**, 927 (2020)
12. R. Gautam, A.S. Bassi, E.K. Yanful, *Appl. Biochem. Biotechnol.* **141**, 85 (2007)
13. H. Chen, L. Kong, Y. Wang, *J. Membr. Sci.* **487**, 109 (2015)
14. J.M. Raquez, Y. Habibi, M. Murariu, P. Dubois, *Prog. Polym. Sci.* **38**, 1504 (2013)
15. P. Bordes, E. Pollet, L. Averous, *Prog. Polym. Sci.* **34**, 125 (2009)
16. M. Irani, H. Ismail, Z. Ahmed, *Polym. Test.* **32**, 502 (2013)
17. J.H. Chang, Y.U. An, G.S. Sur, *J. Polym. Phys. Appl. Sci.* **41**, 94 (2003)
18. A. Oral, M.A. Tasdelen, A.L. Demirel, Y. Yagci, *Polymer* **50**, 3905 (2009)
19. M.A. Tasdelen, W.V. Camp, E. Goethals, P. Dubois, F.D. Prez, Y. Yagci, *Macromolecules* **41**, 6035 (2008)
20. M. Aydin, M.A. Tasdelen, T. Uyar, S. Jockusch, N.J. Turro, Y. Yagci, *J. Polym. Sci. A.* **51**, 1024 (2013)
21. S.S. Ray, K. Yamada, M. Okamoto, Y. Fujimoto, A. Ogami, K. Ueda, *Polymer* **44**, 6633 (2003)
22. A.M. AlGhouti, Y. MAIDegs, *J. Chem. Eng.* **173**, 15 (2011)
23. M. Rafatullah, O. Sulaiman, R. Hashim, A. Anees, *J. Hazard. Mater.* **177**, 70 (2010)
24. C. Jiucun, W. Haodong, L. Wenqian, X. Jiming, Z. Lihui, S. Baoben, *Colloid. Polym. Sci.* **288**, 173 (2010)
25. Z. Zhang, L. Xu, P. Zhou, *Microporous Mesoporous Materials Available* **315**, 110904 (2021)
26. S. Haoue, H. Dardar, M. Belbachir, *Bull. Chem. React. Eng. Catal* **15**(1), 221 (2020)
27. H. Moustafa, S.N. Lawandy, M. Rabee, *Int. J. Adhes. Adhes.* **100**, 102617 (2020)
28. L. Mrah, R. Meghabar, *J. Thermoplas. Compos. Mater.* **2**, 659 (2020)
29. A. Harrane, M. Belbachir, *Macro. Mol. Symp.* **247**, 379 (2007)
30. M. Zahraoui, A. Mokhtar, M. Adjdir, F. Bennabi, R. Khaled, A. Jelad, A. Bengueddach, M. Sassi, *Res. Chem. Intermed.* **45**, 633 (2019)
31. N. Bouchikhi, M. Adjdir, K.C. Bendeddouche, D. Bouazza, A. Mokhtar, F. Bennabi, A. Tabti, A. Sehmi, H. Miloudi, *Mater. Res. Express.* **6**, 12 (2020)
32. Z. Draoua, A. Harrane, M. Belbachir, *J. Macromol. Sci. A.* **52**, 130 (2015)
33. X. Weibing, G. Mingliang, H. Pingsheng, *J. Polym. Sci.* **40**(5), 408 (2002)
34. Q. Yuan, S. Awate, R.D.K. Misra, *J. Eur. Polym. J.* **42**, 1994 (2006)
35. C.R. Tseng, H.Y. Lee, F.C. Chang, *J. Polym. Sci. Polym. Phys. B.* **39**, 2097 (2001)
36. F. Chivrac, E. Pollet, L. Avérous, *J. Polym. Sci. Polym. Phys. B.* **45**, 1503 (2007)
37. M.Jouyandeh, S.M.R. Paran, R.Jannesari A, D.Puglia, M .RezaSaeb (2019) *Prog. Org. Coat.* **131**,333
38. M. Jouyandeh, S.M.R. Paran, A. Jannesari, M.R. Saebi, *Prog. Org. Coat.* **127**, 429 (2019)
39. M.ŞA. Erena, H. Arslanoğlu, H. Çiftçi, *J. Environ. Chem. Eng.* **8**(5), 104247 (2020)
40. I. Fedal, A. Ramdani, S. Taleb, E.M. Gaigneaux, N. Batis, N. Ghaffour, *Desalin. Water Treat.* **52**, 2654 (2014)
41. Y.L. Ma, Z.R. Xu, T. Guo, P. You, *Colloid Interface Sci.* **280**, 283 (2014)
42. H. Cherifi, F. Bentahar, S. Hanini, *Appl. Surf. Sci.* **282**, 52 (2013)
43. D. Kavitha, C. Namasivayam, *Biores. Technol.* **98**, 14 (2007)
44. C.H. Weng, Y.F. Pan, *J. Hazard. Mater.* **144**(1–2), 355 (2007)
45. Y.N.Liu, X.Zhou, X.Wang, K.Liang, Z.K.Yang, C.C.Shen, M. Imran, S.Sahar , A.W0 Xu, *RSC. Adv.* **7**, 30080 (2017)
46. C.H. Giles, D. Smith, A. Huiston, *J. Colloid Interface Sci.* **47**, 755 (1974)
47. J.S. Piccin, L.C.S. Gomes, A. Feris, M. Gutterres, *J. Chem. Eng.* **183**, 30 (2012)
48. A. Ramdani, Z. Taleb, A. Guendouzi, A. Kadeche, H. Herbache, A. Mostefai, S. Taleb, A. Deratani, *Can. J. Chem.* **98**, 79 (2020)

49. A. Ramdani, A. Kadeche, M. Adjdir, Z. Taleb, D. Khou, S. Taleb, A. Deratani, *Water Pract. Technol.* **15**, 130 (2020)
50. J. Baliti, A. Asnaoui, S. Abouarnadasse, *J. Innov. Res. In Adv. Eng.* **1**, 2149 (2014)
51. F. Tikhani, M. Jouyandeh, S.H. Jafari, S. Chabokrow, M. Ghahari, K. Gharanjig, F. Klein, N. Hampp, M.R. Ganjali, K. Formela, M.R. Saeb, *Prog. Org. Coat.* **135**, 176 (2019)
52. Y. Kuang, X. Zhang, S. Zhou, *Water* **587**, 2 (2020)
53. R.M. Firdaus, N.I.M. Rosli, J. Ghanbajaj, *J. Nanopart. Res.* **257**, 21 (2019)
54. M. Peiyong, M. Meina, W. Jinzhou, Q. Yuzhi, W. Dongqiang, Z. Xianwen, *J. Mater. Res.* **34**(17), 3040 (2019)
55. M.S. Jyothi, A.V. Jagadeesha, T.V. Kanakalakshmi, P. Mahesh, R.G. Balakrishna, S. J. *Polym. Environ.* **27**, 2408 (2019)
56. A. Alizadeh, M. Fakhari, Z. Safaei, M. M. Khodeai, E. Repo, A. Asadi (2020) *Inorg. Chem. Commun.* **121** 108204

Publisher's Note Springer Nature remains neutral with regard to jurisdictional claims in published maps and institutional affiliations.

Authors and Affiliations

Zohra Draoua^{1,2} · Amine Harrane^{1,3} · Mehdi Adjdir^{4,5}

¹ Laboratory of Polymer Chemistry, Department of Chemistry, Faculty Exact Sciences, University Oran1 Ahmed Ben Bella, BP 1524 El M'Naouer, 31000 Oran, Algeria

² Department of Civil Engineering, Faculty of Architecture and Civil Engineering, University of Sciences and Technology of Oran Mohamed Boudiaf, USTO-MB, BP 1505, El M'naouer, 31000 Oran, Algeria

³ Department of Chemistry, FSEI University Abdelhamid Ibn Badis Mostaganem, Mostaganem, Algeria

⁴ Laboratory of Applied Organic Synthesis, Faculty of Exact and Applied Sciences, University Oran1 Ahmed BenBella, BP 1524 El M'Naouer, 31000 Oran, Algeria

⁵ Department of Engineering Process, Faculty of Technology, University of Saida, Dr. Moulay Tahar, Saida, Algeria